

PURDUE UNIVERSITY
GRADUATE SCHOOL
Thesis/Dissertation Acceptance

This is to certify that the thesis/dissertation prepared

By Ruwan Janapriya Egoda Gamage

Entitled

A High Resolution 3D and Color Image Acquisition System for Long and Shallow Impressions in Crime Scenes

For the degree of Master of Science

Is approved by the final examining committee:

Mihran Tuceryan

Jiang Yu Zheng

Shiaofen Fang

To the best of my knowledge and as understood by the student in the *Thesis/Dissertation Agreement, Publication Delay, and Certification/Disclaimer (Graduate School Form 32)*, this thesis/dissertation adheres to the provisions of Purdue University's "Policy on Integrity in Research" and the use of copyrighted material.

Mihran Tuceryan

Approved by Major Professor(s): _____

Approved by: Shiaofen Fang

03/17/2014

Head of the Department Graduate Program

Date

A HIGH RESOLUTION 3D AND COLOR IMAGE
ACQUISITION SYSTEM FOR LONG AND SHALLOW IMPRESSIONS
IN CRIME SCENES

A Thesis

Submitted to the Faculty

of

Purdue University

by

Ruwan Janapriya Egoda Gamage

In Partial Fulfillment of the

Requirements for the Degree

of

Master of Science

May 2014

Purdue University

Indianapolis, Indiana

To my wife, *Uthpala*, and our son, *Saniru*.

ACKNOWLEDGMENTS

I would first like to thank my adviser, Professor Mihran Tuceryan, for his valuable and constructive guidance during the planning and development of this research work. Professor Tuceryan is a dedicated adviser, and I'm very lucky to have him as my mentor.

I would like to thank my committee members, Professor Jiang-Yu Zheng and Professor Shiaofen Fang, for agreeing to serve on my committee. In addition, I'm thankful for Professor Zheng's invaluable guidance in this work.

Assistance and resources provided by Mr. Herb Blitzer, to perform device testing, is greatly appreciated.

I would also like to thank Mr. Steve Evers and his team from Macron Dynamics for their assistance in choosing a linear actuator and a motor for the IMPREsS device.

I am particularly grateful for the assistance given by friends to scan impressions even in freezing temperatures. Also, my thanks go to Nicole for her support for purchasing parts for the device.

My heartfelt thanks also go to my parents, sisters, wife and son for their encouragement and endless support over the years of my study.

TABLE OF CONTENTS

	Page
LIST OF TABLES	vi
LIST OF FIGURES	vii
ABBREVIATIONS	viii
ABSTRACT	ix
1 INTRODUCTION	1
1.1 Objectives	1
1.2 Contribution	2
1.3 Organization	2
2 LITERATURE REVIEW	3
3 METHODOLOGY	7
3.1 Hardware construction	7
3.1.1 Linear actuator	8
3.1.2 Programmable motor with gearbox	10
3.1.3 Video camera	10
3.1.4 Power supply	10
3.1.5 Laser stripe lights	10
3.1.6 The prototype	11
3.2 Image processing algorithms	13
3.2.1 Laser stripe detection based on hues	13
3.2.2 Laser stripe detection based on RGB lookup table	15
3.2.3 Color texture image extraction	17
3.3 Calibration of the triangulation configuration	17
3.3.1 Coordinate System Definitions	18
3.3.2 One Time Calibration of the System	19
3.3.3 Vanishing Point of the Linear Motion	20
3.3.4 Calculating the Vanishing Point	22
3.3.5 Computing the pose of the camera	22
3.3.6 Coordinate System Transformation (α - xyz to O - XYZ)	23
3.3.7 Using $Z = f$ Plane for Coordinate Transformation	24
3.3.8 3D Coordinates of the Points on the Calibration Object	24
3.3.9 Finding the laser plane	25
3.4 Calculating the 3D model	26

	Page
4 RESULTS AND DISCUSSION	28
4.1 Results of 3D Scans of Impression Data	28
4.2 Accuracy and Resolution Measurements for the System	30
5 CONCLUSIONS AND FUTURE WORK	39
5.1 Future Work	40
LIST OF REFERENCES	41
APPENDICES	
APPENDIX A USER INTERFACE	44
A.1 Physical Buttons Interface	44
A.2 Tablet PC Controller	44
A.3 Software, Graphical User Interface	44
APPENDIX B COOL MUSCLE PROGRAM	48

LIST OF TABLES

Table	Page
4.1 Physical vs measured absolute errors.	37

LIST OF FIGURES

Figure	Page
2.1 Illustration of Structured Light.	4
2.2 Structured lighting techniques.	5
3.1 The design for the device prototype built.	8
3.2 The camera and two laser configuration.	9
3.3 Two lasers as seen from camera.	9
3.4 The prototype and a close-up of the laser and camcorder assembly. . .	12
3.5 RGB lookup tables for an indoor scan.	16
3.6 Figure showing various coordinate system definitions.	20
3.7 Vanishing point.	20
3.8 How two frames are captured for calibration.	21
4.1 Fused results of red and green laser heightmaps.	29
4.2 Shoe prints scanned in a natural setting.	31
4.3 A long span tire impression scanned with IMPREsS device.	32
4.4 A scan of a shoe impression.	32
4.5 Scan results of a shoe with known characteristics.	33
4.6 Test setup.	34
4.7 Scenarios considered for testing.	35
4.8 Test setup 5th scenario, B is lifted by 40mm.	36
A.1 Buttons to control the device.	45
A.2 Buttons Circuit Diagram.	45
A.3 The tablet PC interface to control the device.	46
A.4 The graphical user interface to capture 3D measurements.	47

ABBREVIATIONS

HD	High Definition
HSV	Hue Saturation and Value
IMPRES	IMPReSSION Evidence Scanning
ME	Mean Error
RGB	Red Green and Blue
ROI	Region of Interest
SD	Standard Deviation
SWGTTREAD	Scientific Working Group for Shoe-print and Tire Tread Evidence

ABSTRACT

Egoda Gamage, Ruwan Janapriya M.S., Purdue University, May 2014. A High Resolution 3D and Color Image Acquisition System for Long and Shallow Impressions in Crime Scenes. Major Professor: Mihran Tuceryan.

In crime scene investigations it is necessary to capture images of impression evidence such as tire track or shoe impressions. Currently, such evidence is captured by taking two-dimensional (2D) color photographs or making a physical cast of the impression in order to capture the three-dimensional (3D) structure of the information. This project aims to build a digitizing device that scans the impression evidence and generates (i) a high resolution three-dimensional (3D) surface image, and (ii) a co-registered two-dimensional (2D) color image. The method is based on active structured lighting methods in order to extract 3D shape information of a surface. A prototype device was built that uses an assembly of two line laser lights and a high-definition video camera that is moved at a precisely controlled and constant speed along a mechanical actuator rail in order to scan the evidence. A prototype software was also developed which implements the image processing, calibration, and surface depth calculations. The methods developed in this project for extracting the digitized 3D surface shape and 2D color images include (i) a self-contained calibration method that eliminates the need for pre-calibration of the device; (ii) the use of two colored line laser lights projected from two different angles to eliminate problems due to occlusions; and (iii) the extraction of high resolution color image of the impression evidence with minimal distortion. The system results in sub-millimeter accuracy in the depth image and a high resolution color image that is registered with the depth image. The system is particularly suitable for high quality images of long tire track impressions without the need for stitching multiple images.

1 INTRODUCTION

In crime scene investigations it is necessary to capture images of impression evidence such as tire track or shoe impressions. Currently, such evidence is captured by taking two-dimensional (2D) color photographs or making a physical cast of the impression in order to capture the three-dimensional (3D) structure of the information [1, 14, 18]. The 2D photographs, under the right illumination conditions, may highlight feature details in the evidence, but do not provide metric depth measurement information for such features. Obtaining a 3D physical cast of the impression may destroy the evidence in the process. Therefore, the use of a 3D imaging device which can capture the details of such impression evidence can be a useful addition to the toolkit of the crime scene investigators (CSI). In this thesis, the design of such an impression imaging device, IMPression Evidence Scanning (IMPRES) device, which includes a calibration method for obtaining the 3D image with the proper metric information is presented. Furthermore, The prototype hardware and the software to scan and calculate 3D digital images of such impression evidence are also developed.

1.1 Objectives

IMPRES device captures 3D impressions without destroying the evidence compared to traditional methods like making casts. The output of the device contains a 3D model and a registered high resolution 2D image. Furthermore, the resultant 3D model and 2D image has sub-millimeter accuracy [10, 9].

The specific objectives of this thesis are :

- Designing and building a novel, inexpensive, portable, and non-destructive method for recording impressions of tire tracks and footwear.

- A resolution of $< 1\text{mm}$ in depth in the digitized depth image.
- Developing the methodology of capturing high-quality digital image of the track along with a three dimensional model.
- Experimentally validating the sub-millimeter accuracy in the digitized image.

1.2 Contribution

This thesis explains the research, design and development of the IMPREsS device. The device can scan and generate 3D data with sub-millimeter accuracy. Furthermore, it provides a registered high resolution color image. It also scans long tire tracks (1.75m) as well as short shoe impression without changing the configuration. Moreover, the IMPREsS device has a self-contained calibration method that eliminates the need for pre-calibration, especially helpful when it is used as a portable device. The device prototype hardware was designed and built in house. Servo motor controller programming and tablet PC programming are also done by our team. In addition, a robust software prototype was developed to calibrate the system, to generate 3D models, to generate 2D color images, and to measure dimensions of scanned objects in metric units.

1.3 Organization

This thesis is organized into eight chapters. Chapter 1 presents introduction, objectives and contributions of this thesis. Chapter 2 reviews existing techniques in detail. Chapter 3 describes the methodology used in designing building the IMPREsS device. Chapter 4 discusses experimental results and description of the method for systematically testing the device accuracy. Chapter 5 presents conclusions and some suggestions for future work to improve the device performance. Finally, the appendix covers some details of the software and hardware interface.

2 LITERATURE REVIEW

The normal process of imaging impression evidence with a 2D photographic camera requires that the camera's optical axis be perpendicular to the ground at the site of the evidence. Also, there is a requirement for proper oblique lighting in order to see details created by varying depths of the impression as intensity variations in the photographs. In the case of tire tracks, where the impression may cover several linear feet, the ground may not be level and camera distances may lead to confusing readings [1, 14, 18]. The requirements for imaging such evidence are specified by the Scientific Working Group for Shoe print and Tire Tread Evidence (SWGTTREAD) guidelines [25]. A device based on principles similar to the one described in this paper has been built before in order to scan relics excavated from archaeological sites and construct their 3D computer models [30, 31]. The device was constructed for measuring tall sculptures and has been brought into a UNESCO World Heritage Site. Calibration of such devices is not trivial [29, 6]. The accuracy requirements of scanning such sculptures, however, are different in scale than the ones for scanning the footprint and tire tread impressions. Typically, the desired features on footprint and tire tread impression evidence are at the sub-millimeter scale and the accuracy of the imaging device should be such that these features are not missed.

Over the years, techniques such as depth from stereo vision, depth from focus, depth from time-of-flight, and depth from structured light have been used in 3D scanning devices. Traditionally, a stereo vision system uses two cameras, displaced along horizontal direction, to retrieve two different views of a scene. By analyzing these two views 3D surface data is generated with the help of common features, such as corners or edges, found in the overlapping region. Depth from focus relies on changing the focus and analyzing the sharpness of points in image frames. This usually is a time consuming approach given many images have to be captured at

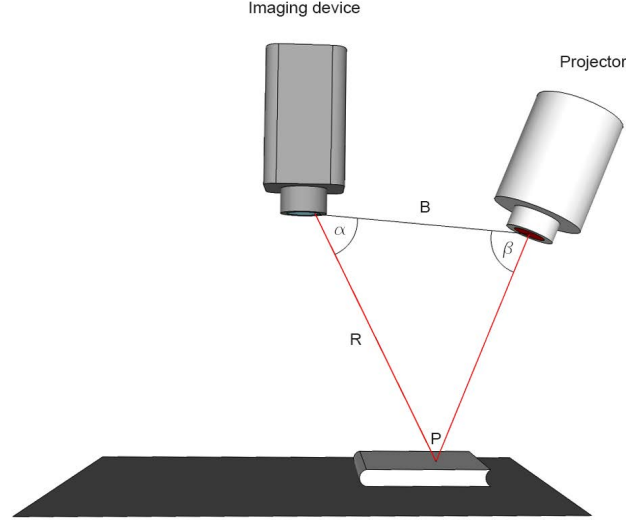


Figure 2.1.: Illustration of Structured Light.

different focal distances. In the time-of-flight method, the time required for a light pulse to travel is measured to calculate distance and eventually the 3D data.

There has been a lot of previous work on structured lighting methods [26]. Figure 2.1 illustrates the structured light concept using a imaging device, such as a video camera, and a structured light projector. To find the 3D coordinates of point P, it is necessary to understand the geometric relationship between the imaging device and the projector. The relationship is given by [11],

$$R = B \frac{\sin \beta}{\sin (\alpha + \beta)} \quad (2.1)$$

As explained in detail in [11], these methods could be divided into two broad categories, sequential and one shot. The sequential category, in which the system captures multiple shots (images) while changing projected patterns, can be further divided into binary code [16, 22](Figure 2.2a), gray code [22, 15](Figure 2.2b), phase shift [27](Figure 2.2c) and combination of gray code and phase shift [13].

The one shot category is further divided into spatially varying patterns, stripe indexing and grid indexing. The Rainbow 3D camera is an example of spatially

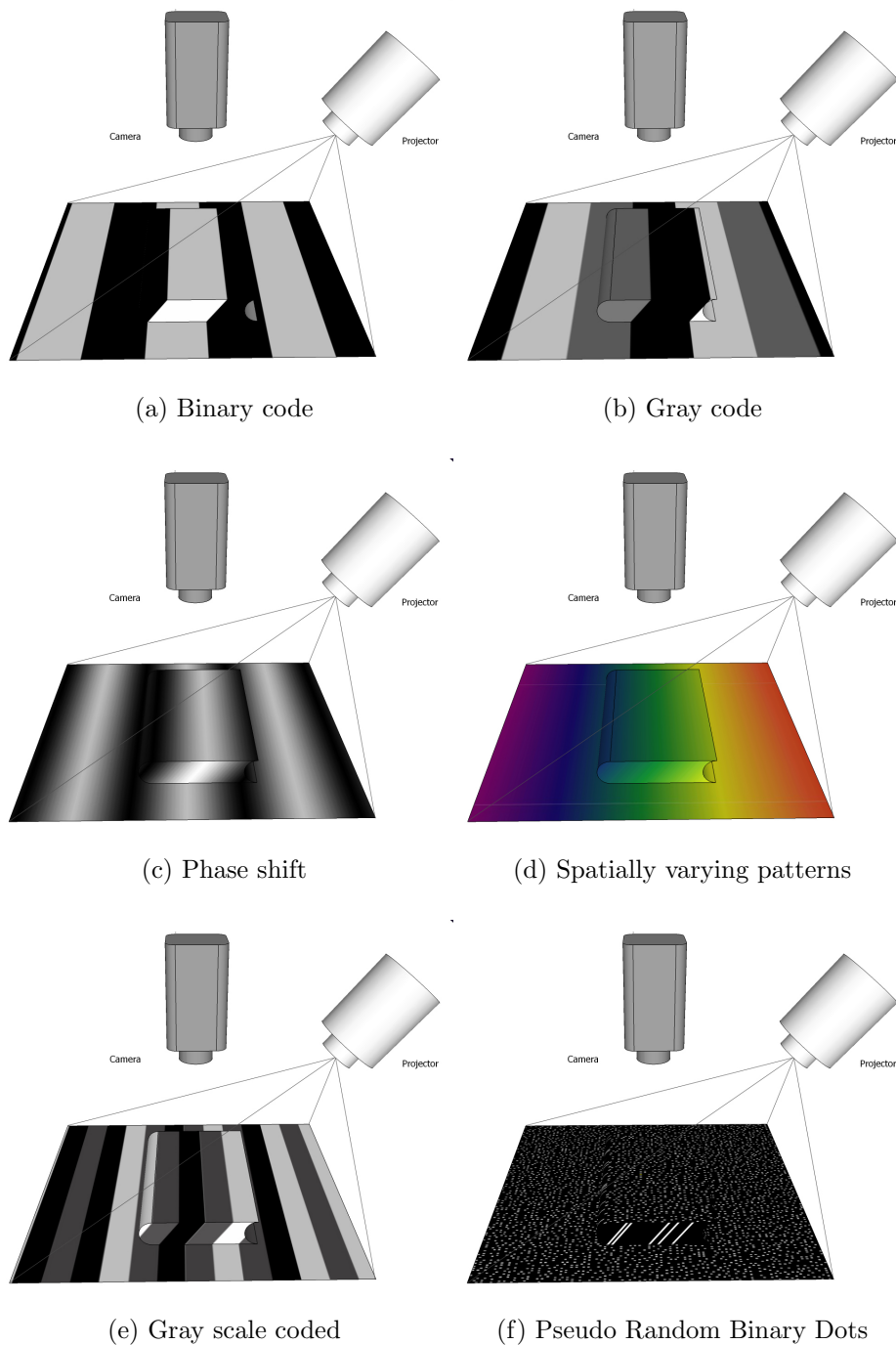


Figure 2.2.: Structured lighting techniques.

varying patterns [12]. As the name suggests this camera projects a spatially varying colors on to the object surface as shown in Figure 2.2d. Given that each projection angle of each color is known, 3D data can be computed easily using straightforward triangulation. Color coded stripes [3], Segmented stripes [17], Gray-scale coded stripes [7](Figure 2.2e) are examples of stripe indexing. Pseudo Random Binary Dots [19](Figure 2.2f), a technique used in the popular Kinect sensor (first generation), is a grid indexing method. Color coded grid [20] is an another example of above method.

Some of these methods rely on solving the correspondence problems [21]. The accuracy characteristics of others do not meet the forensic requirements of impression evidence scanning [2]. In most outdoor applications it is important to implement on-site calibration to avoid miss-alignments during transportation [28].

The current work modifies it to satisfy the special requirements in the field of forensic imaging. Buck et al. present the use of existing commercial 3D imaging devices for footwear impressions [5]. The existing devices do not satisfy some of the imaging requirements (e.g., resolution in depth) in forensics applications. They do not work very well outdoors on long track impressions with a single scan. They usually require multiple short scans which need to be stitched together.

3 METHODOLOGY

The IMPREsS device employs triangulation geometry of a projected line laser light on to a surface and observing its image from a slightly offset position. Generally, this method suffers from the problem of finding corresponding positions between two images. The solution is to perform a sequential scanning and calculating the 3D surface directly for each point on the laser line. The detection of the laser line is done based on its color. This is done for each image frame generated by the camera. Furthermore, color information is also captured to generate a high resolution color image and metric 3D model of the surface.

In the rest of this section, hardware configuration of the device, the various calibration algorithms, and the image processing and 3D surface estimation algorithms are described.

3.1 Hardware construction

The IMPREsS device consists of a linear actuator, a high definition video camera, and, two line laser lights. Green and red color laser lights are used as shown in Figure 3.1. Advantages of using two color lasers are, eliminating the blind spots due to occlusion and easily distinguishing two light sources.

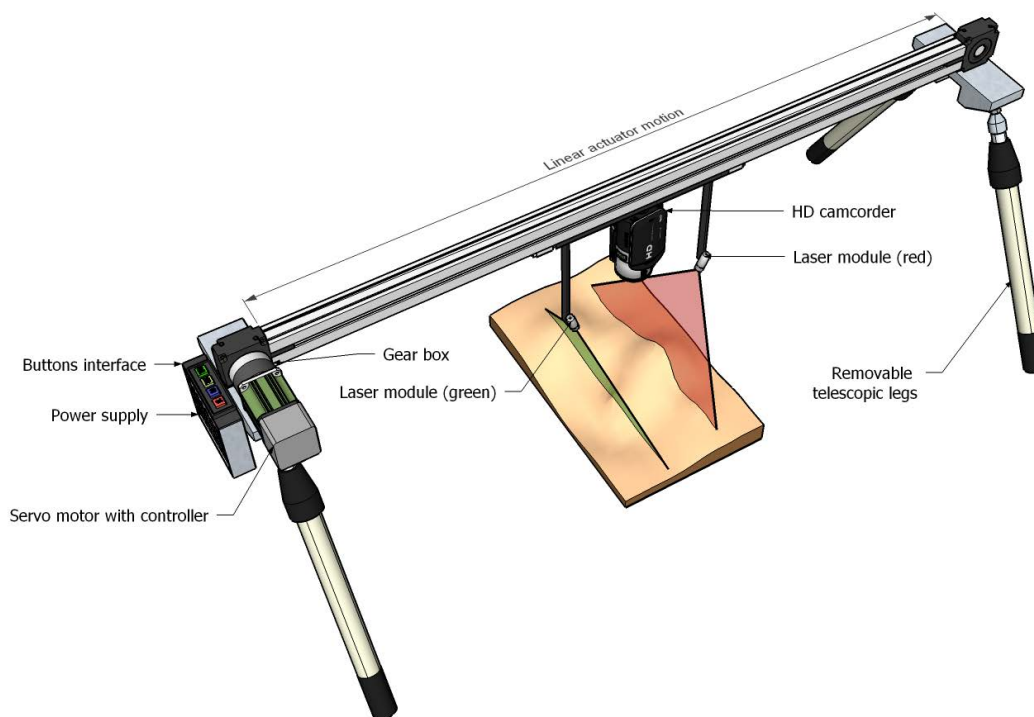


Figure 3.1.: The design for the device prototype built.

3.1.1 Linear actuator

A linear actuator converts rotary motion of a motor into a linear motion. In IMPREsS, a linear actuator was needed to provide linear motion for camera and laser lights assembly. A linear actuator was considered with following characteristics.

1. Higher repeatability
2. Lower weight
3. Higher rigidity
4. Load capacity

Macron Dynamics MSA-PSC linear actuator has higher repeatability given its zero backlash construction. Its load capacity was sufficient to move camera assembly.

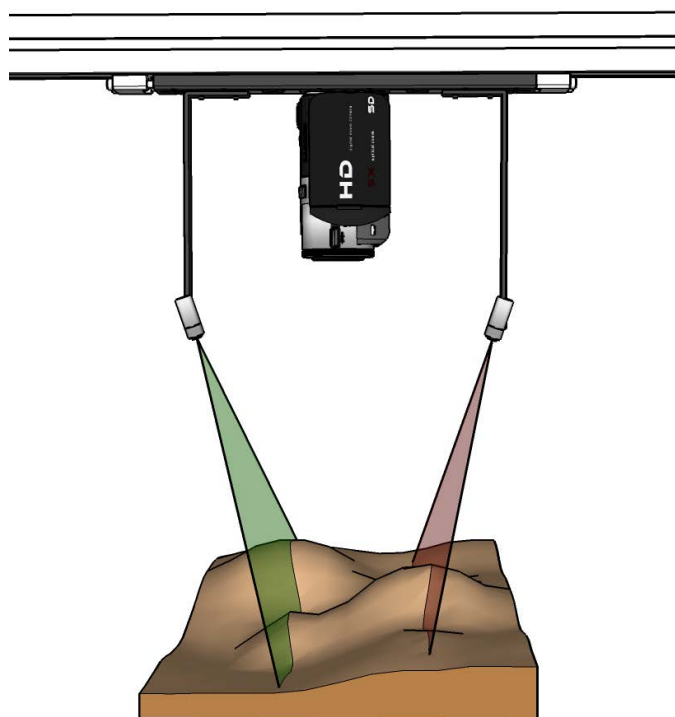


Figure 3.2.: The camera and two laser configuration.

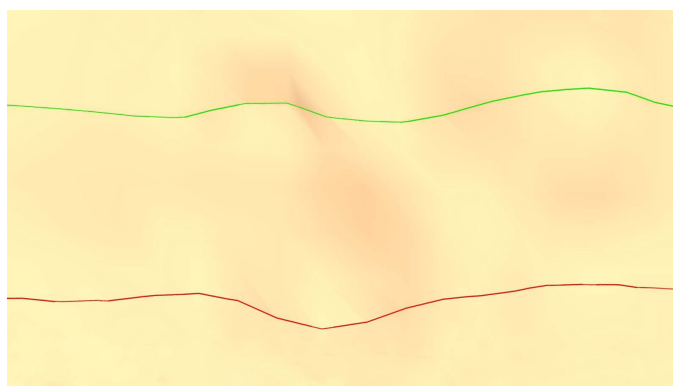


Figure 3.3.: Two lasers as seen from camera.

Its body was made out of Aluminum extrusion, providing higher rigidity and lower weight.

3.1.2 Programmable motor with gearbox

The programmable motor was an integral part of the IMPREsS device. It was required to provide enough torque to support horizontal movement of the camera assembly. Furthermore, accurate constant slow speeds are required to achieve sub-millimeter accuracy in the IMPREsS device. An 8:1 ratio gear box was used to achieve both higher torque requirement and slower speed requirements.

Myostat Cool Muscle (CM1 Series) Integrated Servo motor was used in the IMPREsS device. It also provided programmable serial interface to add controls. The motor was programmed to accept 4 button interface to home, to stop, to scan short distance for shoe impressions, and to scan longer distance for tire impressions. The electronic circuit diagram can be found in Figure A.2. The controller program is found in Appendix A.3.

3.1.3 Video camera

The video camera has to record 1920x1080 full high definition (HD) recording. Furthermore, it should capture frames at 30 frames per second. Considering above the Canon VIXIA HF M30 HD camcorder was selected for the IMPREsS device.

3.1.4 Power supply

The Myostat motor is equipped with a 24V power supply which accepts 110V AC input. To provide portability for the device, a 400W power inverter which can provide 110V output from a motor vehicle was used. In addition, to scan impressions in places where a vehicle couldn't reach, a 600W portable power source was used.

3.1.5 Laser stripe lights

Laser stripe lights were selected based on their power and the characteristics of the laser line. Low power, less than 5mW, Class 3R lasers were used considering laser

safety. Fixed focus laser diodes which generate a thin and a straight laser lines are specifically chosen to improve the accuracy of the overall system. Furthermore, the fan angle was chosen to be greater than the field of view of the camera.

3.1.6 The prototype

The final physical prototype of the device is shown in Figure 3.4. In summary, following components are used to build the device.

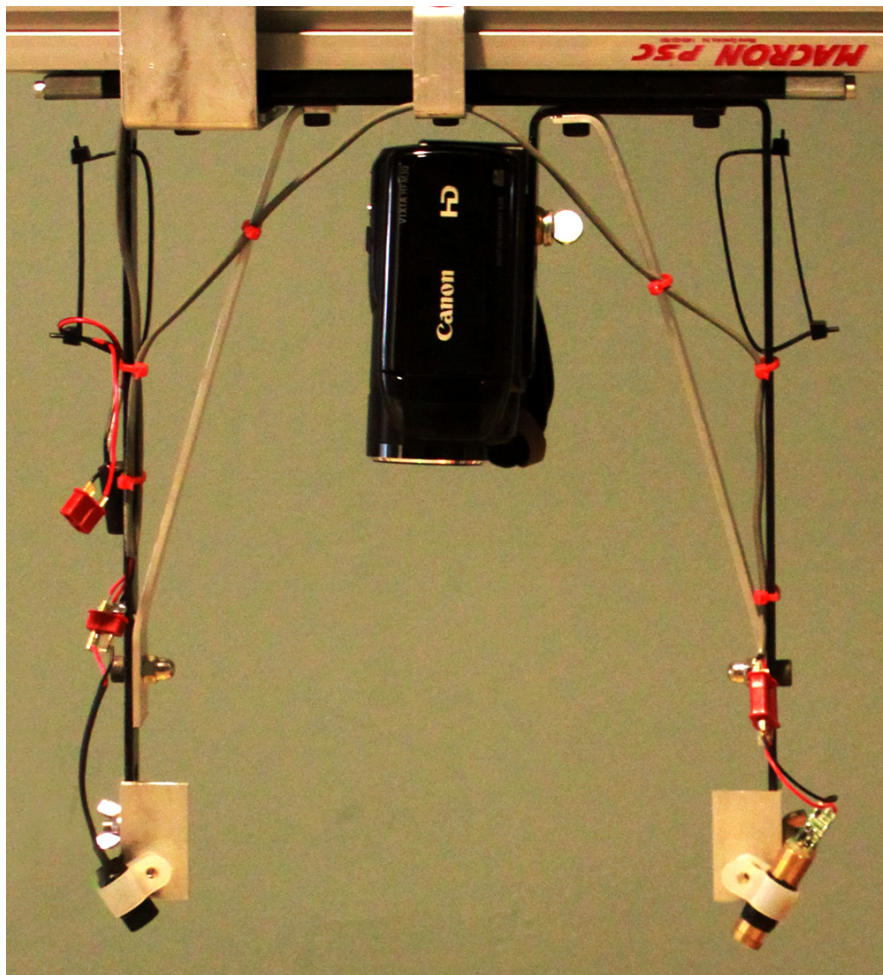
1. Linear actuator: Macron Dynamic belt drive linear actuator MSA-PSC, 1771mm long.
2. Myostat Cool Muscle (CM1 Series) Integrated Servo motor with a planetary gearbox 8:1.
3. 24VDC Power supply and USB programming interface cable
4. Canon VIXIA HF M30, HD camcorder.
5. Laser stripe lights.
 - (a) 5mWatt, 532nm green module.
 - (b) 3mWatt, 650nm red module.

The bracket and a leg assembly on the two sides of the linear actuator were designed and built in such a way that they can be taken off in order to package and carry the device to the field. Moreover, a bracket to mount the camcorder and the laser lights onto the linear actuator with a fixed geometric configuration was also developed.

The device was designed to be portable by one person. It has a total weight of 5kg, and can be loaded in to a normal van or a pick-up truck. It's legs are also removable for easy transportation. It has four buttons preprogrammed to operate the device. The buttons are, (1) home to a preset position, (2) stop, (3) do a long scan (170cm), and (4) do a short scan (50cm).



(a)



(b)

Figure 3.4.: The prototype and a close-up of the laser and camcorder assembly.

The device is powered from a vehicle power outlet or from a portable battery unit. The camera focus and exposure are set to manual mode at the beginning of the scan. This is done to eliminate the possibility of the camera's optical parameters changing during the scanning process.

A user interface for controlling the device has been developed on a PC as well as on a mobile tablet using the Android platform. This interface allows the field technician to control an expanded set of scan parameters such as linear actuator speed, start and stop positions, and/or scan length in a more customized way than the four preset buttons. A more advanced user interface may also allow in the future the capability of changing the preset values of these buttons.

The video of two laser stripes are recorded into a flash disc. After the scan of the entire site is done, the disc is moved to a PC in the crime lab and the video clips are copied to the hard disc of PC for image processing, 3D reconstruction, and further analysis.

3.2 Image processing algorithms

A combination of two color based laser stripe detection techniques are used to detect laser line in each video frame. The first method is based on Hue and the second method is based on a RGB lookup table.

3.2.1 Laser stripe detection based on hues

The detection of the laser stripe in the image is based on the color properties of the pixels. The detection of the laser stripes is done by restricting the search to a smaller region of interest (ROI) in the video frame which is determined by the camera/laser configuration and a limit on surface variations.

The search ROI is aimed at reducing the search region for detecting the laser light in the image. This search region is determined by the amount of variation in surface height, which in turn has a direct effect on the deformation of the laser line in the

image. If the surface variation is not large (is shallow) as in a typical impression evidence surface, the deformation of the laser line will be small. Therefore, the search for detecting the laser light can be restricted to a small subregion of the image.

This search ROI is also determined by the angle with which the laser light is projected on the surface with respect to the camera capturing the images. One laser light is projected somewhere in the upper half of the image and the second laser light will be projected somewhere in the lower half of the image. Thus for each laser light, a search ROI is defined based on this *a priori* knowledge of the device configuration. Once the ROI is defined, the laser stripe is detected by using a Hue-Saturation-Value (HSV) representation of the image. This identification is done if the pixel's hue value falls within a specified range $[\text{hue}_{\min}, \text{hue}_{\max}]$, which is determined by the color of the particular laser light. A dilate morphological image operation is performed in the vertical direction. The pixels resulting from this operation constitute a set of candidate points for the laser pixels. This set of pixels typically forms a thick (5-10 pixels wide) band and the location of the laser stripe needs to be refined for better accuracy.

In the mask generated based on the hue field, in each vertical line, a peak of the intensity values is searched. These peaks are the pixels with the maximum Value (brightness) for the pixel in the HSV representation and correspond to the peak of the laser stripe.

Laser edge information is also combined to improve accuracy of peak intensity method. The edge detection is carried out only in a region (a band) closer to detected peak location of laser intensity. A vertical edge operator is used to detect horizontal edges. Resulting leading and trailing edges of the laser stripe are used for further processing. The midpoint of the leading and trailing edge is calculated and if it is within a certain distance of the peak location, the midpoint is marked as the laser location.

3.2.2 Laser stripe detection based on RGB lookup table

To further improve the robustness of the laser stripe detection, a slightly modified method based on an adaptively constructed RGB lookup table [24] was implemented. This approach relies on learning the color distribution of the background image and detects a pixel as a laser light if it falls outside the parameters of this background color distribution. This approach contains four image processing steps.

- *Stripe edge detection:* First using the red channel of the image, edges of red laser is detected using Sobel edge filter. Similarly, green channel is used of the image for detecting green laser. The resultant image has pixels highlighting horizontal edges of the laser stripe. Next, an another step is performed with a high and low thresholds to eliminate noise and low response edges. All pixels are initially assumed to be part of laser stripe which lie in between a negative and a positive edge.
- *RGB lookup table based color validation:* To validate pixels in a laser stripe, two lookup tables are generated, one for green laser light and another for red laser light. The lookup table consists of color values belonging to the *background color subspace*(bcs). To generate a lookup table, all pixels c_i outside of the corresponding laser detection ROI of every 100th frame are considered. Here $c_i = (R, G, B) \in ([0, 255], [0, 255], [0, 255])$, where the square brackets indicate ranges in the three color bands. Let's consider the lookup table: bcs_{red} for red laser. First, a complement lookup table, $\overline{bcs}_{red}(R, G, B)$ is constructed as follows:

$$\overline{bcs}_{red}(R, G, B) = \begin{cases} 1 & \text{if } \exists i : (R, G, B) \in c_i \text{ or } (R = 0) \\ 0 & \text{otherwise} \end{cases} \quad (3.1)$$

Then, $\overline{bcs}_{red}(R, G, B)$ is used to construct the actual lookup table $bcs_{red}(R, G, B)$ as follows:

$$bcs_{red}(R, G, B) = \begin{cases} 1 & \text{if } \exists R' \geq R : \overline{bcs}_{red}(R', G, B) = 1 \\ 0 & \text{otherwise} \end{cases} \quad (3.2)$$

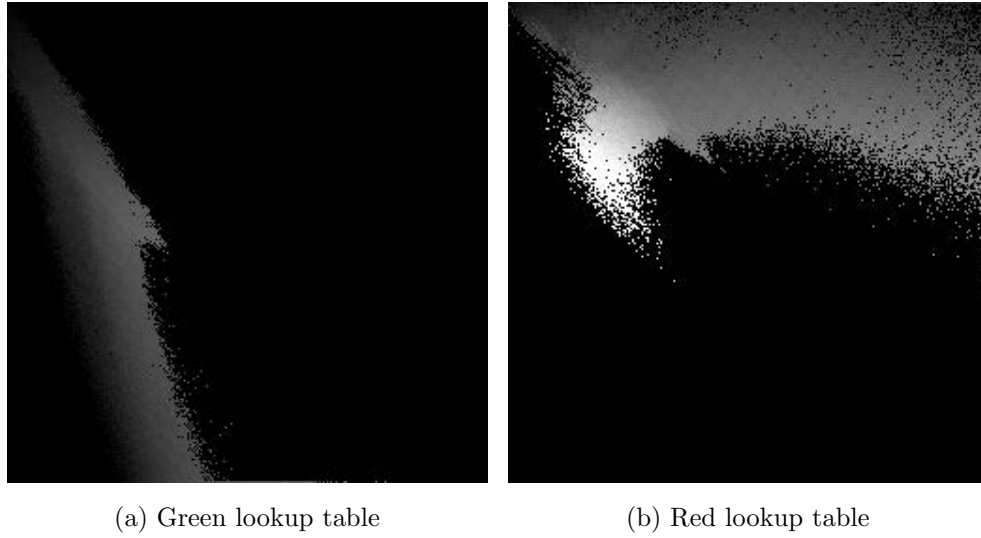


Figure 3.5.: RGB lookup tables for an indoor scan.

A given color pixel $x_i = (r, g, b)$ is classified as a pixel belong to red laser stripe, if $bcs_{red}(r, g, b) = 0$. If a stripe from the edge detection step contains more than 95% of laser pixels, it is considered as a valid laser stripe. Similarly green laser is also validated.

Figure 3.5 shows lookup tables as images of an indoor scan. Figure 3.5a shows the lookup table for green laser as an image. Red and green channels are represented in horizontal and vertical axis of the image. The image has 255x255 dimensions and intensity represents green channel which ranges from 0 to 255.

- *Stripe width validation:* Each stripe width is validated using a higher threshold and a lower threshold. The lower threshold is set to 2 pixels and higher threshold is set to 20 pixels. These numbers provided more signal to noise ratio during testing.
- *Peak estimation:* Center of mass method [8] is used to determine the peak position of stripe in sub-pixel accuracy :

$$y_{peak} = \frac{\sum_{i=m}^{m+w} iI(i)}{\sum_{i=m}^{m+w} I(i)} \quad (3.3)$$

where i is the starting row of the laser stripe and w is the width of the detected laser stripe and $I(i)$ is the intensity of that particular color channel at pixel i in each column.

3.2.3 Color texture image extraction

A high resolution color image of the impression evidence is also extracted , simultaneously with the laser stripe detection. This is done by extracting the image line perpendicular to the scanner motion direction in the middle of each video frame. The color image captured by this process has following properties:

- The spatial resolution of the image along the scan direction is dependent on the speed with which the linear actuator moves. Therefore, the resolution along this direction can be increased by scanning the impression using a slower motion of the actuator. Since the video is being captured at a fixed rate of 30 frames per second, the distance between the scan lines of successive video frames will be smaller as the actuator moves more slowly. The image formed along the scan direction is an orthographic projection determined by the scan motion.
- In the direction perpendicular to the scan motion, the resolution is a perspective projection with the spatial resolution determined by the highest resolution of the HD camcorder. The size of a highest resolution video is 1920×1080 pixels. In order to maximize the resolution of the resulting image, the camcorder is oriented such that the highest resolution dimension of the video frames (i.e., 1920 pixels) is perpendicular to the actuator motion.

3.3 Calibration of the triangulation configuration

To calibrate the IMPREsS device an L-shaped calibration object is used, as shown in Figure 3.8. The calibration object is required to precisely compute the geometric

configuration of the laser beams and the camera in order to generate the 3D model. The system captures the calibration object in at least one on-site scanning task, i.e., when it's first taken off the truck and set up. This eliminates the risk that a pre-calibrated configuration can be invalidated during the transportation and set-up of the device. Instead, the scanning of the evidence and calibration of the configuration is self-contained and the only requirement in the field is that the criminalist places the calibration object in the scene for the first scan.

The speed of the camera-laser configuration, is one of the parameters of the device that is used in the calibration and that also affects the resolution. Since the camera is capturing 30 frames per second constantly, the highest resolution 3D model can be obtained when the linear actuator is moving at the slowest speed.

The speed (v mm/s) of the linear actuator was measured when it was moving. The camera calibration gives the focal length (i.e. f) in pixel units. The system currently operates in its slowest speed of 1.3138 mm/s.

Calibration of the camera is performed [4] in order to correct for lens distortion at widest zoom angle settings, and found that f is 2110 in pixel units. Moreover, radial distortion correction is applied to every image frame captured from the camera and this corrected image is used for all subsequent depth calculations.

A vanishing point method is used to find the pose of the camera with respect to the linear actuator. Then the calibration object is used as seen in the image to calculate the orientations of the red and green laser planes. Everything, including the points on the evidence surface is eventually calculated in a single coordinate system which is defined by the linear actuator. The details of each of these calculations are described below.

3.3.1 Coordinate System Definitions

Three main coordinate systems are used(see Figure 3.6).

1. $o-xyz$: original image camera coordinate system. Coordinates are measured in pixel units after calibration of camera intrinsic parameters.
2. $O-XYZ$: ideal image coordinate system. The coordinate system after correcting roll and tilt. Y axis is parallel to linear actuator. Coordinates are in pixel units.
3. $O'-X'Y'Z'$: linear actuator-based 3D world coordinate system. The coordinate system axes are parallel to the axes of ideal image coordinate system. Coordinates are in metric units.

3.3.2 One Time Calibration of the System

First an off-line calibration is performed to estimate the optical properties and radial distortion of the camera. This is done for the camera once at the beginning to obtain the intrinsic camera parameters such as focal length (in pixels), camera center position, and radial distortion. This assumes that during the scan the camera zoom is fixed. This calibration can also be performed in the lab in advance if the zoom factor is determined to be fixed at widest angle and confirmed at the camera buttons before the scanning takes place. This calibration can even be done only once if the same camera is used for a long period. This is different than calibrating the camera and laser light geometric configuration which is done as an integrated part of the scans and is described in more detail in Sections 3.3.3 to 3.3.9.

The camera calibration uses a standard function in the OpenCV software package. A checkerboard grid pattern is shown to the camera at different angles. Several frames with different poses of the board are captured by the camera. The software detects the corners and computes the camera focal length, optical center in the image frame, and the radial distortion parameters of the lens. With these parameters, an image can be transformed to the $o-xyz$ coordinate system.

The motor translation speeds are also measured in the lab. Using the camera to shoot the moving assembly through two specified positions on the linear actuator, we

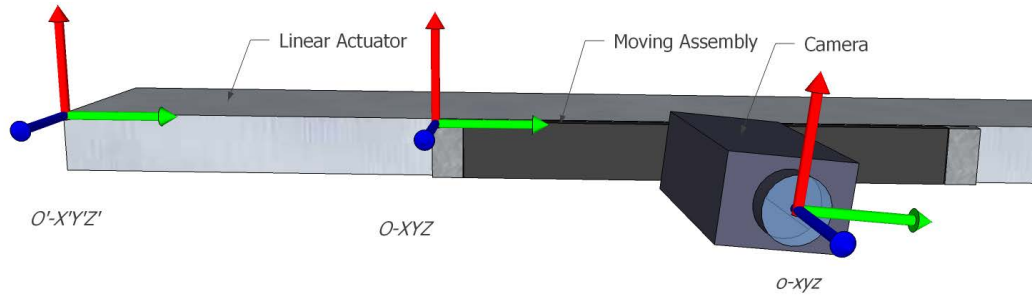


Figure 3.6.: Figure showing various coordinate system definitions.

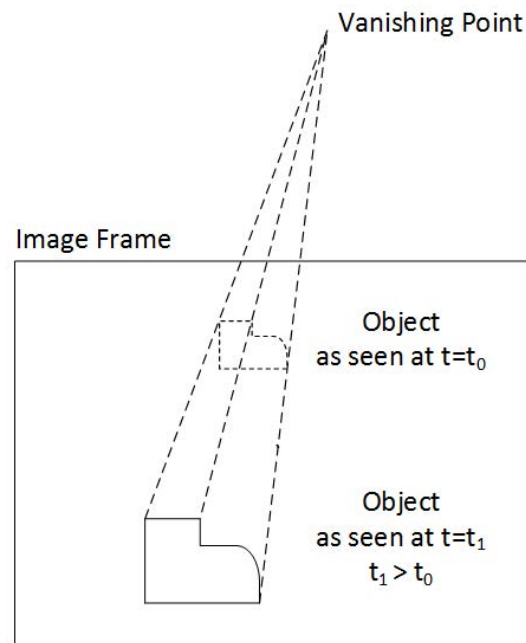


Figure 3.7.: Vanishing point.

can calculate the precise translation velocity of the cart (excluding the accelerating and stopping periods) by counting the video frames (each frame takes 1/30 sec).

3.3.3 Vanishing Point of the Linear Motion

Ideally, the camera should be connected to the linear actuator as shown in Figure 3.1, looking downward and the y-axis of the image aligned perfectly with the

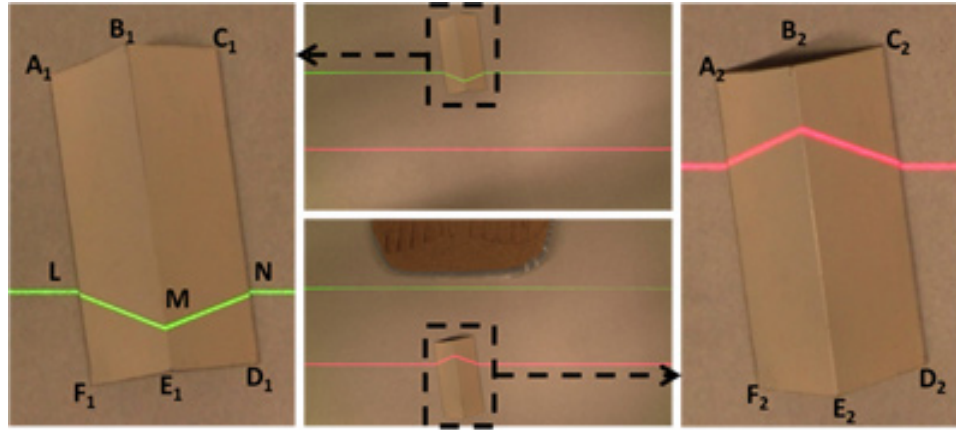


Figure 3.8.: How two frames are captured for calibration.

linear actuator's direction of motion. Achieving this physically, however, is not realistic. Therefore, we assume the camera is put on the linear actuator roughly as described above and the small misalignments are accounted for via a calibration procedure. This calibration calculates the exact pose of the camera with respect to the linear actuator coordinate system. The calibration object is placed in the scene roughly pointing in the direction of the linear actuator motion. Assume the camera is perfectly aligned with the linear actuator coordinate system. If we translate the camera along the linear actuator and take two images, one before and one after the translation, corresponding points on the calibration object in the two images will form parallel lines. This will result in a vanishing point formed by the lines at infinity. In reality, the camera is not perfectly aligned with the linear actuator system resulting in the vanishing point to be finite as seen in Figure 3.7. This fact is used to estimate the camera pose with respect to the linear actuator coordinate system from the calculated vanishing point.

Two frames are captured as seen in Figure 3.8, one at $t = t_1$ when the green laser is projected onto the calibration object and the second at $t = t_2$ when the red laser is projected onto the calibration object. Corners of the calibration object, $(A_i, B_i, C_i, D_i, E_i, F_i, \text{ for } i = 1, 2)$, are marked using an interactive interface devel-

oped in the software. Usually, the person doing the computations in the crime lab pick these points. The following are the steps for achieving this calibration.

3.3.4 Calculating the Vanishing Point

The lines with which the vanishing points are calculated are defined by two sets of corresponding points between the two frames captured during the camera motion. One set of corresponding points are A_1 and A_2 , and the other set is C_1 and C_2 . Let the line A_1A_2 be $y = m_1x + c_1$ and the line C_1C_2 be $y = m_2x + c_2$. Consider only the x and y pixel locations of A_1, A_2, C_1 , and C_2 , and by computing the intersection we obtain the vanishing point (x_v, y_v) .

$$\begin{pmatrix} 1 & -m_1 \\ 1 & -m_2 \end{pmatrix} \begin{pmatrix} x_v \\ y_v \end{pmatrix} = \begin{pmatrix} c_1 \\ c_2 \end{pmatrix} \quad (3.4)$$

From which we obtain

$$\begin{pmatrix} x_v \\ y_v \end{pmatrix} = \begin{pmatrix} 1 & -m_1 \\ 1 & -m_2 \end{pmatrix}^{-1} \begin{pmatrix} c_1 \\ c_2 \end{pmatrix} \quad (3.5)$$

3.3.5 Computing the pose of the camera

Computing the pose with respect to O-XYZ is done using the vanishing point as follows.

Camera roll (θ) around its optical axis is given by,

$$\theta = \tan^{-1} \left(\frac{x_v}{y_v} \right) \quad (3.6)$$

Camera tilt (α) between optical axis and the line goes through the optical center and also perpendicular to linear motion.

$$\alpha = \frac{y_v}{|y_v|} \tan^{-1} \left(\frac{f}{\sqrt{x_v^2 + y_v^2}} \right) \quad (3.7)$$

3.3.6 Coordinate System Transformation (o-xyz to O-XYZ)

Let the vector x be the coordinates of a point in o-xyz and the vector X be the coordinates of a point in O-XYZ.

The goal is to transform all quantities into the ideal coordinate system This is given by the following equations:

$$\mathbf{X} = \mathbf{R}_x(\alpha)\mathbf{R}_z(\theta)\mathbf{x} \quad (3.8)$$

Equation (3.6), gives the roll angle in CW direction. It is required to rotate the coordinate system CCW by this angle. Therefore,

$$\mathbf{R}_z(\theta) = \begin{pmatrix} \cos \theta & -\sin \theta & 0 & 0 \\ \sin \theta & \cos \theta & 0 & 0 \\ 0 & 0 & 1 & 0 \\ 0 & 0 & 0 & 1 \end{pmatrix} \quad (3.9)$$

Equation (3.7), gives the tilt angle in CCW direction. It is required to rotate the coordinate system CW by this angle. Therefore,

$$\mathbf{R}_x(\alpha) = \begin{pmatrix} 1 & 0 & 0 & 0 \\ 1 & \cos \alpha & \sin \alpha & 0 \\ 0 & -\sin \alpha & \cos \alpha & 0 \\ 0 & 0 & 0 & 1 \end{pmatrix} \quad (3.10)$$

Therefore the total transformation matrix, \mathbf{T} , for correcting the roll and tilt, is given by

$$\mathbf{T} = \begin{pmatrix} 1 & 0 & 0 & 0 \\ 1 & \cos \alpha & \sin \alpha & 0 \\ 0 & -\sin \alpha & \cos \alpha & 0 \\ 0 & 0 & 0 & 1 \end{pmatrix} \begin{pmatrix} \cos \theta & -\sin \theta & 0 & 0 \\ \sin \theta & \cos \theta & 0 & 0 \\ 0 & 0 & 1 & 0 \\ 0 & 0 & 0 & 1 \end{pmatrix} \quad (3.11)$$

3.3.7 Using $Z = f$ Plane for Coordinate Transformation

Transforming A_1 and A_2 to corresponding ideal image coordinate systems when $t = t_1$ and $t = t_2$, respectively.

$$\begin{pmatrix} X_{a_1} \\ Y_{a_1} \\ Z_{a_1} \\ 1 \end{pmatrix} = \mathbf{T} \begin{pmatrix} x_{a_1} \\ y_{a_1} \\ z_{a_1} \\ 1 \end{pmatrix} \quad \begin{pmatrix} X_{a_2} \\ Y_{a_2} \\ Z_{a_2} \\ 1 \end{pmatrix} = \mathbf{T} \begin{pmatrix} x_{a_2} \\ y_{a_2} \\ z_{a_2} \\ 1 \end{pmatrix} \quad (3.12)$$

After the roll and tilt correction is applied, the transformed coordinates of the points A_i may not be parallel to the motion direction. Therefore, these points are projected to a plane parallel to the motion direction. The $Z = f$ plane is considered for this operation. A ray from the origin (camera's optical center) via the point in the ideal image coordinate system is used for calculation.

Considering the first frame, i.e., when $t = t_1$,

$$\frac{Z_{a_1}}{f} = \frac{Y_{a_1}}{Y} \quad (3.13)$$

and

$$\frac{Z_{a_1}}{f} = \frac{X_{a_1}}{X} \quad (3.14)$$

Therefore, the projection of A_1 onto the $Z = f$ plane, denoted by A_{1f} , is

$$A_{1f} \equiv \left(\frac{X_{a_1}}{Z_{a_1}} f, \frac{Y_{a_1}}{Z_{a_1}} f, f \right) \quad (3.15)$$

Similarly, the projection of A_2 onto the $Z = f$ plane, denoted by A_{2f} , is

$$A_{2f} \equiv \left(\frac{X_{a_2}}{Z_{a_2}} f, \frac{Y_{a_2}}{Z_{a_2}} f, f \right) \quad (3.16)$$

3.3.8 3D Coordinates of the Points on the Calibration Object

By using two frames with a certain interval on the linear actuator, 3D position in linear actuator coordinate system ($O'-X'Y'Z'$) of a sample point covered by both frames can be estimated. Assuming the distance traveled between the first frame (at

time $t = t_1$) and the second frame (at time $t = t_2$) as d (in metric units) using similar triangles, the Z value for point A in the linear actuator coordinate system can be computed by:

$$\frac{Z'}{f} = \frac{d}{\left(\frac{Y_{a2}}{Z_{a2}}f - \frac{Y_{a1}}{Z_{a1}}f\right)} \quad (3.17)$$

and, therefore,

$$Z' = \frac{d}{\left(\frac{Y_{a2}}{Z_{a2}} - \frac{Y_{a1}}{Z_{a1}}\right)} \quad (3.18)$$

Now considering edges of a triangle the X and Y coordinates of the points can be calculated,

$$\frac{Z_{a1}}{Z'} = \frac{X_{a1}}{X'} \quad (3.19)$$

Also,

$$\frac{Z_{a1}}{Z'} = \frac{Y_{a1}}{Y'} \quad (3.20)$$

Therefore, the coordinates of the point A_1 at time $t = t_1$ are given by:

$$A'_1 \equiv \left(\frac{X_{a1}}{Z_{a1}}Z', \frac{Y_{a1}}{Z_{a1}}Z', Z' \right) \quad (3.21)$$

Points corresponding to B_1, C_1, D_1, E_1 , and F_1 are similarly computed in the linear actuator coordinate system. The position and pose of the calibration object is completely known. The accuracy of the positions is further improved using the physical dimensions of the calibration object.

3.3.9 Finding the laser plane

Let's consider the green laser plane. First, the pixel locations of L , M , and N (in Figure 3.8) are transformed to the ideal image coordinate system using Equation (3.8).

Rays are projected, starting from optical center, through all transformed points. Next, the intersection of the ray and calibration object edges is computed to find the points where laser touches the calibration object. Since edges are in linear actuator

coordinate system, laser points are in linear actuator coordinate system. Finally, using these points, green laser plane is computed.

Red laser plane is also computed using the same method with the red laser points analogous to L , M , and N . All the steps above is repeated for coordinates systems when $t = t_2$.

Assume a point on the laser plane is \mathbf{P}_a , and its surface normal is \mathbf{N} , using the vectors \overrightarrow{LM} and \overrightarrow{MN} we have the equation of the laser plane normal given as the cross-product:

$$\mathbf{N} = \overrightarrow{LM} \times \overrightarrow{MN} \quad (3.22)$$

And the equation of the laser plane, for any point \mathbf{P} on it, is given by the dot-product:

$$\mathbf{N} \cdot (\mathbf{P} - \mathbf{P}_a) = 0 \quad (3.23)$$

3.4 Calculating the 3D model

Each detected laser pixel (x, y) in a frame, is transformed to the ideal image coordinate system. Through that point a ray is projected starting from the optical center. The ideal image coordinate system and the linear actuator coordinate system share the same axes and origin, but they may be at a different scale. Therefore, finding the intersection of the ray and a laser plane gives a linear actuator coordinate of the laser pixel directly.

By applying the offset between red and green laser coordinate systems, i.e. the translation transformation is along y axis — d as in Equation (3.18), red laser plane is brought to $t = t_1$ linear actuator coordinate system. This way, a ray and laser plane intersections always provide registered results for both red and green lasers points. This makes the later fusion of the two 3D models easier.

For any point \mathbf{P} on the laser plane (lit by the laser stripe), its 3D position satisfies:

$$\mathbf{N} \cdot (\mathbf{P} - \mathbf{P}_a) = 0 \quad (3.24)$$

$$\mathbf{N} \cdot \left(\left(\frac{X(t)Z'}{f}, \frac{Y(t)Z'}{f}, Z' \right) - \mathbf{P}_a \right) = 0 \quad (3.25)$$

where \mathbf{P}_a is a point on the laser plane. From this, Z' can be computed as

$$Z' = f \frac{\mathbf{N} \cdot \mathbf{P}_a}{\mathbf{N} \cdot (X(t), Y(t), f)} \quad (3.26)$$

and

$$X' = X(t) \frac{\mathbf{N} \cdot \mathbf{P}_a}{\mathbf{N} \cdot (X(t), Y(t), f)} \quad (3.27)$$

$$Y' = Y(t) \frac{\mathbf{N} \cdot \mathbf{P}_a}{\mathbf{N} \cdot (X(t), Y(t), f)} + tV \quad (3.28)$$

where V is the camera translation speed and t is time. The depth calculation is performed in a lookup table so that the 3D transformation from the image coordinates can be performed much faster.

Finally the 3D model is constructed by considering all laser pixels.

In all *heightmap* 3D models found in the results section, the z value is mapped into 0-255 range of 8-bit gray level intensity in order to allow viewing the results in common image viewing software such as Adobe Photoshop or Gimp. The 3D model has a resolution of (7500 × 7500) where each pixel corresponds to 0.1mm in size. One intensity level in the depth map corresponds to 0.1mm, and the coarsest level for looking at the global elevation changes starts from 10mm. Sometimes, the detailed variations in surface height may be easier to see if we use a pseudo-color mapping of the the height as shown in Figure 4.5.

The color *texture map* of the scanned part has also the same resolution, stored in another image with points exactly corresponding to the ones in the height map. The user can compare height map and the color texture map images to find the shapes of the impression unrevealed in the texture map due to the color and lighting on the ground, and confirm the depth on strange shapes by examining the color texture image.

The prototype software, however, stores 3D models as real number valued point cloud in a binary data file. They also include color texture information. These data files can be used for further processing, such as pattern matching, using the actual metric information.

4 RESULTS AND DISCUSSION

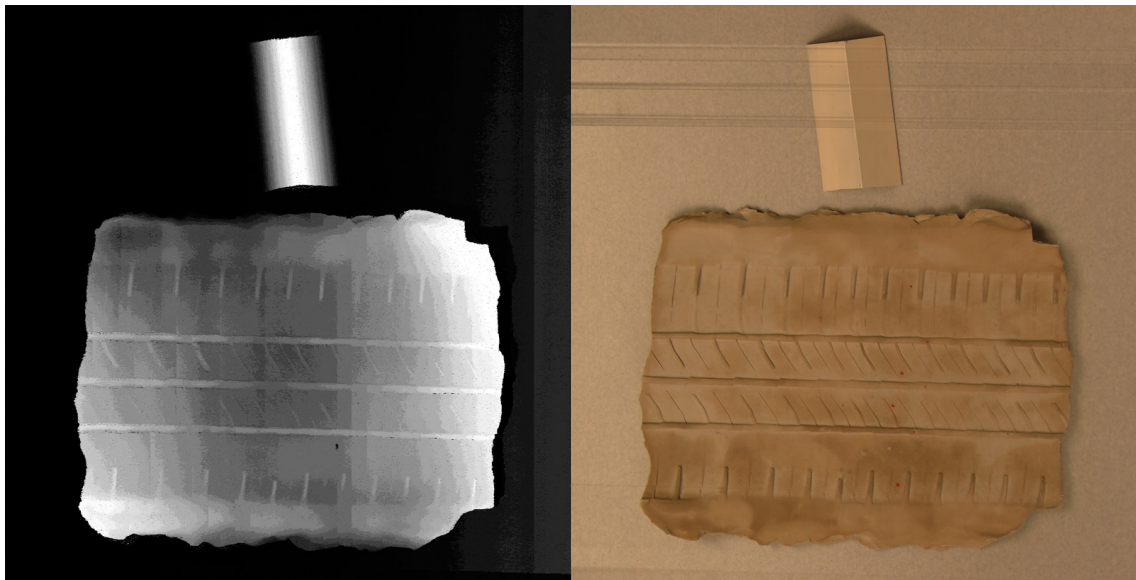
In order to test the IMPREsS device, numerous scans of real impressions were done. Furthermore, a systematic method for testing and accuracy of the device and the resulting depth images was devised.

4.1 Results of 3D Scans of Impression Data

As impression testing experiments, a cast of a tire impression, a tire tread impression on soil, as well as multiple shoe impressions were scanned. Individual test cases are described below.

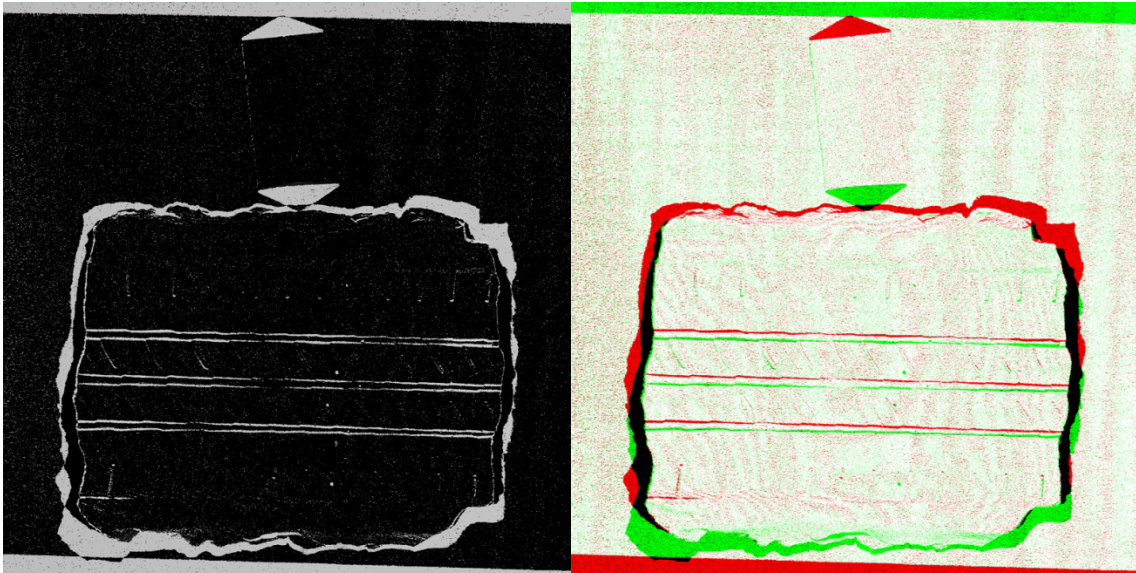
First, a tire cast with the calibration object in the scene was scanned. The HD video file from which these heightmap images are computed consists of a total of 11,146 frames captured in 371.533 seconds. The total size of the video is approximately 1.03 GB and each frame in the video has a resolution of 1920×1088 pixels.

From the results of the calibration described above, a heightmap is computed at each pixel in the image for the two lasers separately. Finally, these separately computed heightmaps are fused into one single heightmap image. This results in filling the missing height data in the occluded regions using the alternate heightmap. Since all coordinates are in a single coordinate system, the estimation of the fused height data is done easily. The final fused results are shown in Figure 4.1. To demonstrate the effectiveness of using two lasers in completing the missing data, the difference between the two registered heightmaps from the green and red lasers are shown in Figure 4.1. As shown Figure 4.1c two heightmaps agree in most of the pixels (therefore, the difference in those pixels is 0). The difference is big in pixels where one image has height data and the other has no height data due to occlusions. In those locations, the fusion fills with the appropriate value. Finally, from the scanned video,



(a) Enhanced heightmap

(b) Registered Texture



(c) Per pixel laser differences

(d) Per pixel contributions of each laser

Figure 4.1.: Fused results of red and green laser heightmaps.

a high resolution texture image is extracted and correctly aligned with the computed, fused heightmap. This result is shown in Figure 4.1b.

Some other images in more natural settings at a linear actuator speed of 13.138 mm/s were also scanned. For example, Figure 4.2 shows a shoe print scanned on a lawn. The color texture images are also shown in Figure 4.2b. Some more 3D scan results are shown in Figure 4.3 and Figure 4.4. In these pictures, the height range is adjusted to the 8-bit gray level range in order to make the features visible.

As another validation test for IMPREsS device, a domain expert and criminalist from SWGTREAD was consulted regarding the capabilities of IMPREsS scan device. As part of this interaction, he has graciously helped to determine what features criminalists would like to detect. He provided a sample shoe and an image of its sole with all the features marked that he would like to see detected in the impression scan. The shoe sole was scanned with the device as shown in Figure 4.5. In this figure the heights are mapped to pseudo color in order to make the height changes more visible. The smaller heights in this picture are closer to the camera. In this test, whether the algorithm can detect known characteristics found on a shoe is specifically checked as shown in Figure 4.5a. Ten known characteristics of the shoe print is shown in the Figure 4.5b. Five out of ten characteristics are visible in Figure 4.5c. Most of the remaining characteristics are visible in the texture image found in Figure 4.5d.

4.2 Accuracy and Resolution Measurements for the System

As part of the validation of IMPREsS device, a systematic accuracy test for the acquired depth images was devised. Figure 4.6a shows the test setup that was used to determine the accuracy. First, wooden blocks with known physical dimensions were created. Next, those blocks were embedded onto two dental stone plates: plate A and plate B. Targets 1, 5, 7 & 9 have a series of slots that vary in width from about 1/4 inch (6.35mm) to 1/32 inch (0.83mm). There is 1/4 inch (6.35mm) between each

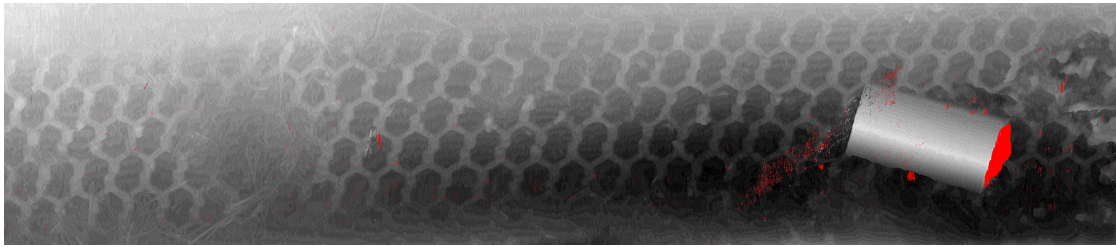


(a) Heightmap of shoeprints



(b) Texture image. The image was acquired during night time. This causes color values that noisy.

Figure 4.2.: Shoe prints scanned in a natural setting.



(a) Heightmap. z range: 307.1mm, 259.2mm.



(b) Color Texture

Figure 4.3.: A long span tire impression scanned with IMPREsS device.

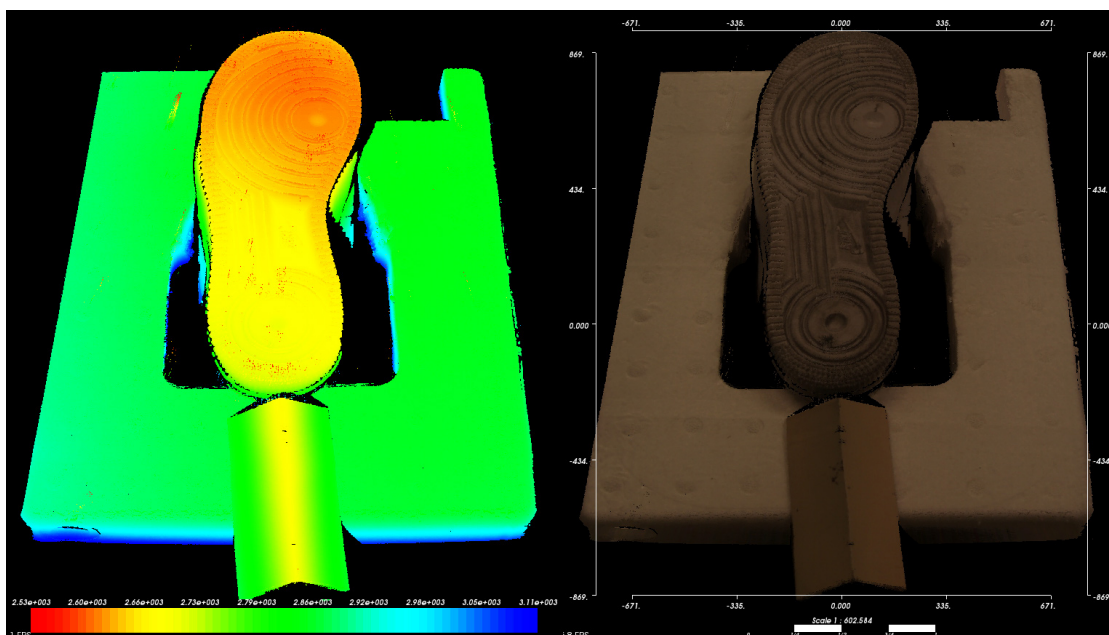


(a) Heightmap. z range: 313.5mm, 280.0mm.

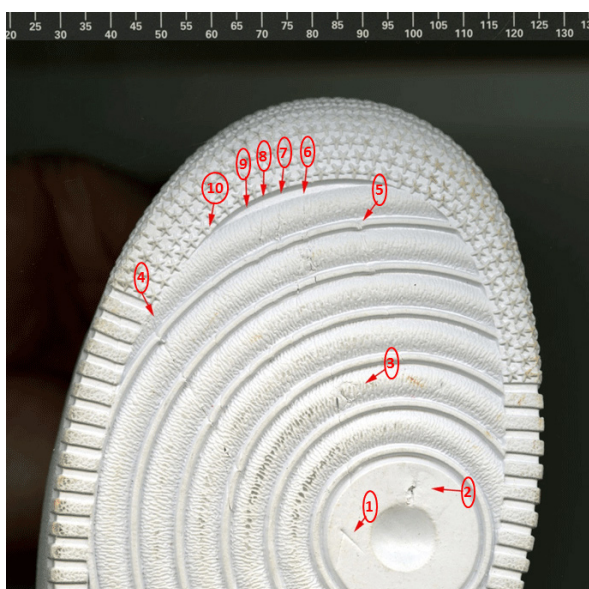


(b) A part of video frame with lasers

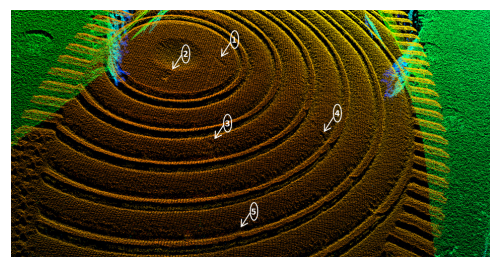
Figure 4.4.: A scan of a shoe impression.



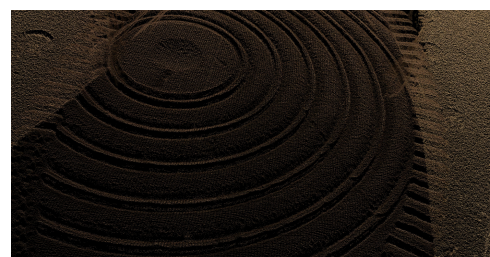
(a) 3D point cloud result of the shoe scan. Left: Color encoded along z axis (colors toward red are closer and colors toward blue are farther to the camera) Right: Texture added.



(b) Points of interest provided by expert.



(c) z axis encoded with pseudocolor.



(d) Color texture applied.

Figure 4.5.: Scan results of a shoe with known characteristics.

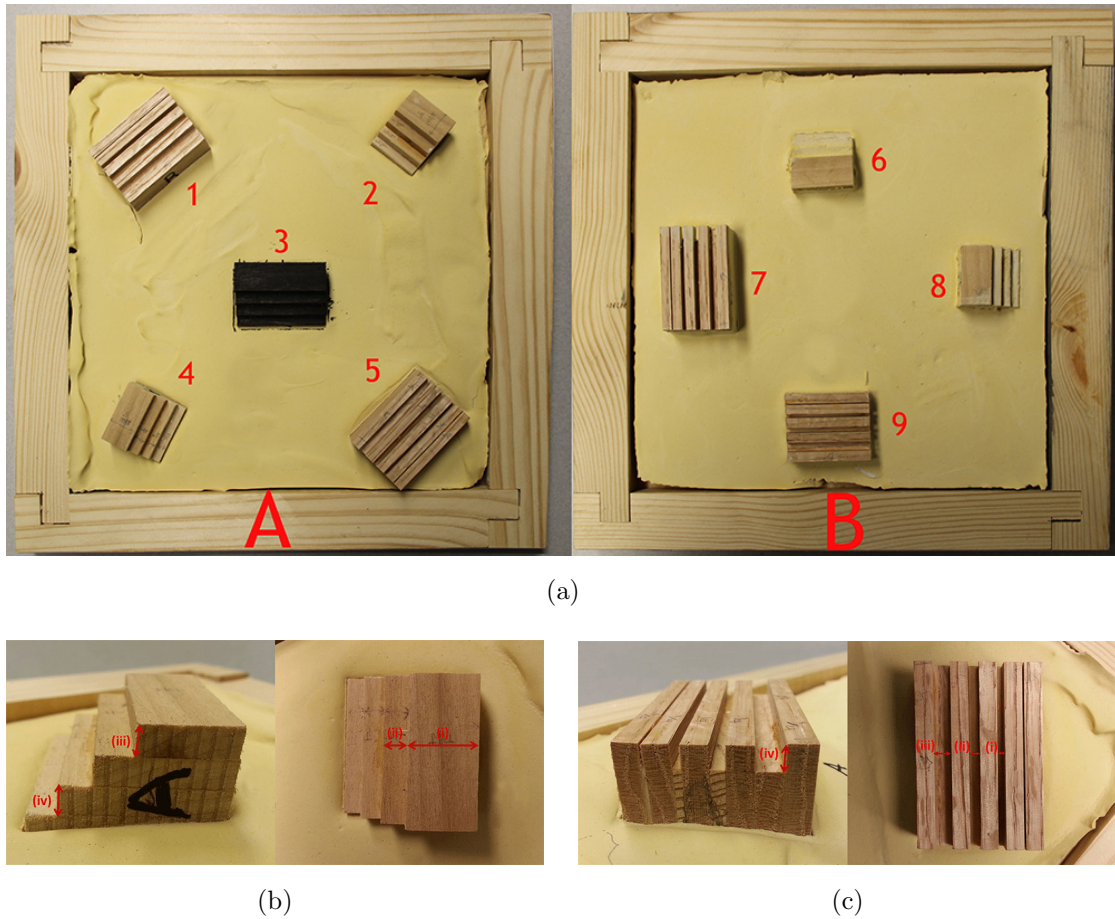


Figure 4.6.: Test setup.

slot. The other targets are each a series of steps, with each step 1/4 inch (6.35mm) wide and 1/4 inch (6.35mm) high.

Following scenarios were considered for testing (Figure 4.7). These scenarios were also meant to assess whether the achieved depth accuracy is location dependent.

1. Plates were positioned in the sequence of A followed by B.
2. Plates were positioned in the sequence of A followed by B, but each rotated by 90 degrees.
3. Plates were positioned in the sequence of B followed by A.

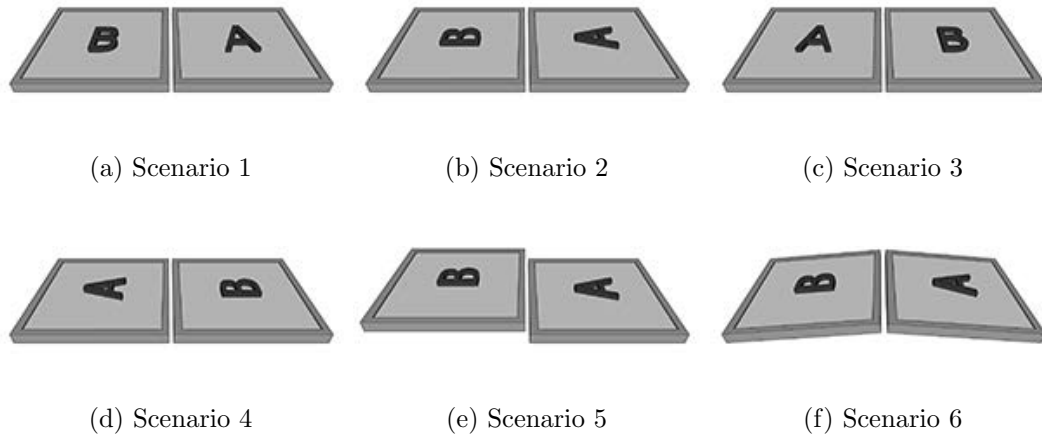
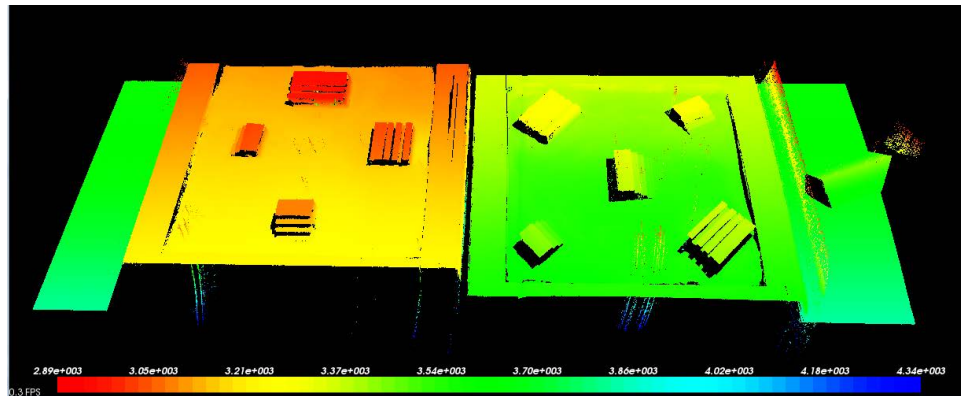


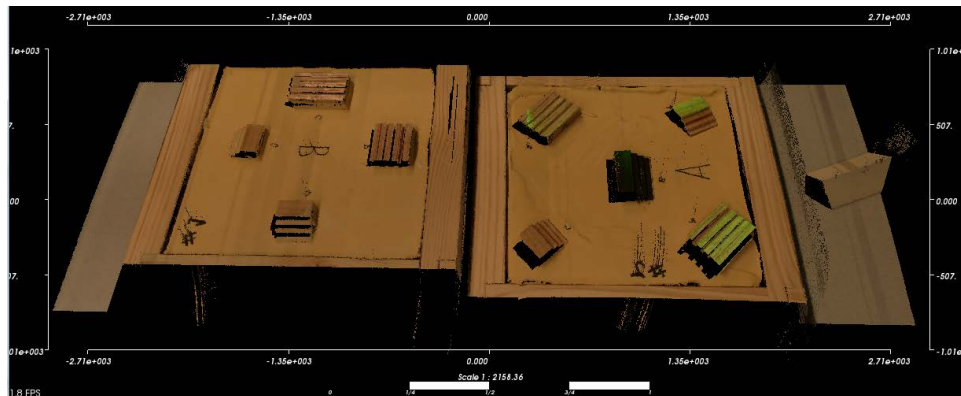
Figure 4.7.: Scenarios considered for testing.

4. Plates were positioned in the sequence of B followed by A, but each rotated by 90 degrees.
5. Plates were positioned in the sequence of A followed by B, but B is lifted 40mm above the surface of A (Figure: 4.8).
6. Plates were positioned in the sequence of A followed by B, but both plates tilted by 5 degrees.

In each of the above scenarios, 4 measurements were done for each wooden block in the generated 3D model. Those 4 measurements are shown in Figure 4.6b and Figure 4.6c. As it can be seen, some measurements were along xy plane, and other measurements were along z axis. Physical dimensions of wooden blocks were also measured by using a vernier caliper. The resulting absolute error amounts between the measured physical dimensions and those computed from the scanned 3D model were used to calculate means and standard deviations. Table 4.1 gives the error statistics (means and standard deviations) of the 208 readings as well as separate statistics for the different test case scenarios. These error statistics were calculated separately for measurements along the xy plane and along the z axis (depth).



(a) 3D Model, Color encoded along z axis.



(b) Texture.

Figure 4.8.: Test setup 5th scenario, B is lifted by 40mm.

Table 4.1: Physical vs measured absolute errors.

	xy ME (mm)	xy SD (mm)	z ME (mm)	z SD (mm)
Order AB	0.54	0.34	1.45	0.47
Order AB, Each Rotated 90 degrees	0.74	0.36	1.55	0.34
Order AB, B lifted by 40mm	0.57	0.48	0.78	0.31
Order AB, Tilted each by 5.035 degrees	0.56	0.36	0.78	0.32
Order BA	0.63	0.36	0.52	0.23
OrderBA, Rotated each 90 degrees	0.6	0.4	0.67	0.31
Overall	0.6	0.39	0.94	0.51

Following accuracy measurements were determined for the system:

- Video camera: frames per second (fps) = 30, focal length (f) = 2110 pixels.
- Linear Actuator Speeds in pulses per second (pps) as indicated by motor controller. The pps speed setting corresponds to the following metric speeds:
- For the widest angle of lens corresponding to the lowest image resolution, it was observed empirically that device can resolve 0.5mm in Z' values as reflected in detectable differences of at least 1 pixel in the disparity image computed. With the increasing zoom value (determined by f), the accuracy can be increased to a much higher level because the camera can have up to 10 times zoom. However, this increased zooming may narrow down the field of view.
- At the lowest linear actuator speed, the device takes approximately 20 minutes to scan a 1.75m long surface. Processing takes around 1 hour in a eight core Intel® Core™ i7-2700 3.5GHz / 16 GB RAM machine.

Processing time depends on the speed the camera moves on the linear actuator. For a short scan of 500mm, the slowest speed (1.3138 mm/s) result in highest resolutions along the scan direction with the ability to detect smaller features in the impression. At this speed, however, the computational times were larger (20 minutes) to process the data in order to generate the 3D image. Conversely, higher linear actuator speeds such as 5.2552 mm/s and 13.138 mm/s resulted resolution but faster computational times of 5 and 2 minutes respectively.

5 CONCLUSIONS AND FUTURE WORK

In conclusion, IMPREsS, an inexpensive high resolution 3D impression device for digitizing footwear and tire impressions in crime scenes was developed. The device achieves a sub-millimeter accuracy in depth images, which seems to be sufficient for most impression evidence needs. Unlike some methods such as physical casting, the method does not destroy the evidence. The photographic technique requires careful attention to many special issues and the casting of impressions is a science of its own—especially in difficult media such as loose sand or snow. In such difficult situations, the resolution is limited with the angle of repose in these materials [23, page 315]. The device is portable with minimal weight.

The device costs about as much as an accessorized digital camera with an associated laptop computer. This cost is much less than commercially available stand-alone laser range finders in the market.

In addition to building the hardware of the device, the software and a calibration method was developed. Furthermore, the calibration method is integrated in the scanning process eliminates the requirement of pre-calibrating the system which can become stale in the field due to the pre-calibrated configuration being changed during transportation and setup. Moreover, two different colored line laser modules are used to eliminate difficulties due to occlusions.

With the 3D depth data, investigators can further have the depth of the impression on soft ground, in addition to the traditional impression that has usually been thresholded to binary shape marks that indicate contact points on the ground. The information upon which comparisons are based becomes richer with proper metric measurements. The scanning times and computation times compare favorably to existing methods of taking casts of the impressions.

5.1 Future Work

The calibration process of IMPREsS contains a user interaction step to capture 6 corner points of the calibration object. This process could be made easier by providing a snap-to-edge feature in the software. This can be achieved by using edge features of the image. Furthermore, if detecting corner points (points of interest) is completely automated user interaction can be avoided. The calibration object could be equipped with fiducial markers to make it easier for automated points of interest detection.

The IMPREsS device robustness can be further improved by introducing controlled lighting. A cover could be developed to eliminate ambient lighting and to provide a controlled light source. Furthermore, the camera of the device can be changed so that the processing is done in real-time. If real-time processing is available, the motion of the linear actuator could be controlled by the computer to perform multiple scans of the regions where higher accuracy is needed.

LIST OF REFERENCES

LIST OF REFERENCES

- [1] W. Bodziak. *Footwear impression evidence: detection, recovery, and examination*. CRC Press, 1999.
- [2] T. Botterill, S. Mills, and R. Green. Design and calibration of a hybrid computer vision and structured light 3D imaging system. In *Proc. 5th Int Automation, Robotics and Applications (ICARA) Conf*, pages 441–446, 2011.
- [3] K. Boyer and A. Kak. Color-encoded structured light for rapid active ranging. *Pattern Analysis and Machine Intelligence, IEEE Transactions on*, PAMI-9(1):14–28, Jan 1987.
- [4] G. Bradski, A. Kaehler, and V. Pisarevsky. Learning-based computer vision with opencv. *Intel Technology Journal*, 9, 2005.
- [5] U. Buck, N. Albertini, S. Naether, and M. J. Thali. 3D documentation of footwear impressions and tyre tracks in snow with high resolution optical surface scanning. *Forensic Science International*, 171(2-3):157 – 164, 2007.
- [6] C. Chen and A. Kak. Modeling and calibration of a structured light scanner for 3-D robot vision. In *Proc. IEEE Int. Conf. Robotics and Automation*, volume 4, pages 807–815, 1987.
- [7] N. Durdle, J. Thayyoor, and V. Raso. An improved structured light technique for surface reconstruction of the human trunk. In *Electrical and Computer Engineering, 1998. IEEE Canadian Conference on*, volume 2, pages 874–877 vol.2, May 1998.
- [8] R. B. Fisher and D. K. Naidu. A Comparison of Algorithms for Subpixel Peak Detection. In *Image Technology, Advances in Image Processing, Multimedia and Machine Vision*, pages 385–404. Springer-Verlag, 1996.
- [9] R. Gamage, A. Joshi, J. Y. Zheng, and M. Tuceryan. A high resolution 3d tire and footprint impression acquisition for forensics applications. In *Applications of Computer Vision (WACV), 2013 IEEE Workshop on*, pages 317–322, Jan 2013.
- [10] R. E. Gamage, A. Joshi, J. Zheng, and M. Tuceryan. A 3d impression acquisition system for forensic applications. In X. Jiang, O. Bellon, D. Goldgof, and T. Oishi, editors, *Advances in Depth Image Analysis and Applications*, volume 7854 of *Lecture Notes in Computer Science*, pages 9–20. Springer Berlin Heidelberg, 2013.
- [11] J. Geng. Structured-light 3d surface imaging: a tutorial. *Adv. Opt. Photon.*, 3(2):128–160, Jun 2011.
- [12] Z. J. Geng. Rainbow three-dimensional camera: new concept of high-speed three-dimensional vision systems. *Optical Engineering*, 35:376–383, Feb. 1996.

- [13] J. Ghring, C. Brenner, J. Bhm, and D. Fritsch. Data processing and calibration of a cross-pattern stripe projector. In *ISPRS Congress*, pages 327–338, 2000.
- [14] M. Houck and J. Siegel. *Fundamentals of forensic science*. Academic Press, 2nd edition, 2010.
- [15] S. Inokuchi, K. Sato, and F. Matsuda. Range imaging system for 3-d object recognition. In *International Conference on Pattern Recognition*, 1984.
- [16] I. Ishii, K. Yamamoto, K. Doi, and T. Tsuji. High-speed 3d image acquisition using coded structured light projection. In *Intelligent Robots and Systems, 2007. IROS 2007. IEEE/RSJ International Conference on*, pages 925–930, Oct 2007.
- [17] M. Maruyama and S. Abe. Range sensing by projecting multi-slits with random cuts. In *Industrial Applications of Machine Intelligence and Vision, 1989., International Workshop on*, pages 163–168, Apr 1989.
- [18] P. McDonald. *Tire imprint evidence*. CRC Press, 1992.
- [19] H. Morita, K. Yajima, and S. Sakata. Reconstruction of surfaces of 3-d objects by m-array pattern projection method. In *Computer Vision., Second International Conference on*, pages 468–473, Dec 1988.
- [20] J. Pags, J. Salvi, and C. Matabosch. Robust segmentation and decoding of a grid pattern for structured light. In F. J. P. Lpez, A. C. Campilho, N. P. de la Blanca, and A. Sanfeliu, editors, *IbPRIA*, volume 2652 of *Lecture Notes in Computer Science*, pages 689–696. Springer, 2003.
- [21] M. Pardonge, B. Walravens, M. Demeyere, K. T. Duy, R. Olszewski, H. Rey-chler, B. Raucant, and C. Eugene. 3D Reconstitution of Dentition by Laser Triangulation Under Structured Lighting. In *Proc. IEEE Int. Workshop Medical Measurement and Applications MEMEA '07*, pages 1–4, 2007.
- [22] J. Posdamer and M. Altschuler. Surface measurement by space-encoded projected beam systems. *Computer Graphics and Image Processing*, 18(1):1 – 17, 1982.
- [23] G. Ranjan and A. Rao. *Basic and Applied Soil Mechanics*. New Age International, 2007.
- [24] K. Strobl, W. Sepp, E. Wahl, T. Bodenmuller, M. Suppa, J. Seara, and G. Hirzinger. The DLR multisensory Hand-Guided Device: the Laser Stripe Profiler. In *Robotics and Automation, 2004. Proceedings. ICRA '04. 2004 IEEE International Conference on*, volume 2, pages 1927 – 1932 Vol.2, 26-may 1, 2004.
- [25] SWGTREAD. SWGTREAD Guidelines. <http://www.swgtread.org/>, 2013.
- [26] Y. F. Wang and A. Pandey. Interpretation of 3D structure and motion using structured lighting. In *Proc. Workshop Interpretation of 3D Scenes*, pages 84–90, 1989.
- [27] C. Wust and D. Capson. Surface profile measurement using color fringe projection. *Machine Vision and Applications*, 4(3):193–203, 1991.

- [28] M. Zhang and D. Li. An on-site calibration technique for line structured light 3D scanner. In *Proc. Asia-Pacific Conf. Computational Intelligence and Industrial Applications PACIIA 2009*, volume 2, pages 30–33, 2009.
- [29] F. Zheng and B. Kong. Calibration of linear structured light system by planar checkerboard. In *Proc. Int Information Acquisition Conf*, pages 344–346, 2004.
- [30] J. Zheng and Zhong Li Zhang. Virtual recovery of excavated relics. *Computer Graphics and Applications, IEEE*, 19(3):6 –11, may/jun 1999.
- [31] J. Y. Zheng. A flexible laser range sensor based on spatial-temporal analysis. In *Pattern Recognition, 2000. Proceedings. 15th International Conference on*, volume 4, pages 740 –743 vol.4, 2000.

APPENDICES

APPENDIX A USER INTERFACE

In order for the field practitioner to operate the device and perform a scan, two different methods of user interface are implemented.

A.1 Physical Buttons Interface

The first method is based on four physical buttons (Figure A.1) on the device whose functions are pre-defined. These functions and the number of buttons is limited by the hardware interface of the actuator but makes the device and interaction with it self-contained.

The electronic circuit diagram supporting above buttons is shown in Figure A.2.

A.2 Tablet PC Controller

The second method is a wireless control through a tablet PC(Figure A.3) with which the field practitioner can interact with the device. This method provides more flexibility and allows the practitioner to change parameters (e.g., linear actuator motion speed) through a software interface.

A.3 Software, Graphical User Interface

A Software application is developed to calibrate device, to process video and to measure 3D data. Technologies, Visual C# .NET and Visual C++ are used to develop the software prototype. Furthermore, following libraries are also used for the implementation.

- OpenCV : For video and image processing routines.



Figure A.1.: Buttons to control the device.

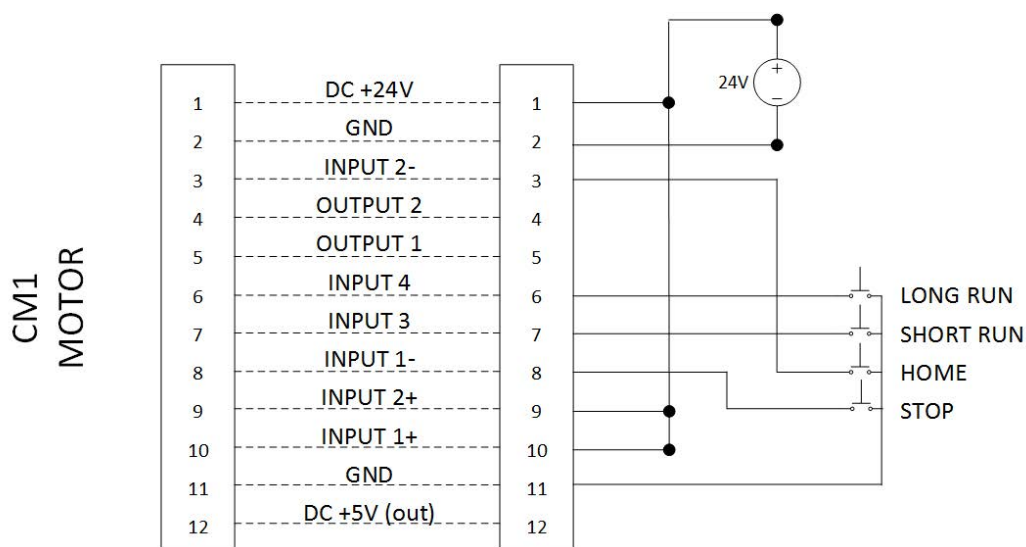


Figure A.2.: Buttons Circuit Diagram.

- Intel Threading Building Blocks : For multi-core programming.
- Point Cloud Library : For processing and visualizing 3D point cloud data.

The software consists of easy to use tools to view and to take 3D measurements as shown in Figure A.4. Using the blue ruler, metric distances between two points

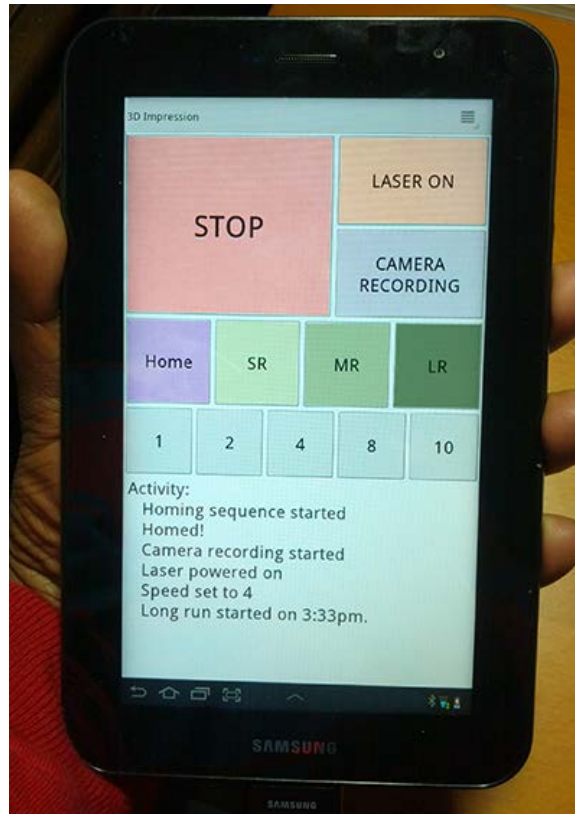


Figure A.3.: The tablet PC interface to control the device.

can be measured in the scanned image. In addition, a 1D profile of the depth values along this blue line is plotted along with a tool for measuring depth/height values precisely. The vertical bars in the figure are points where the laser was not detected.

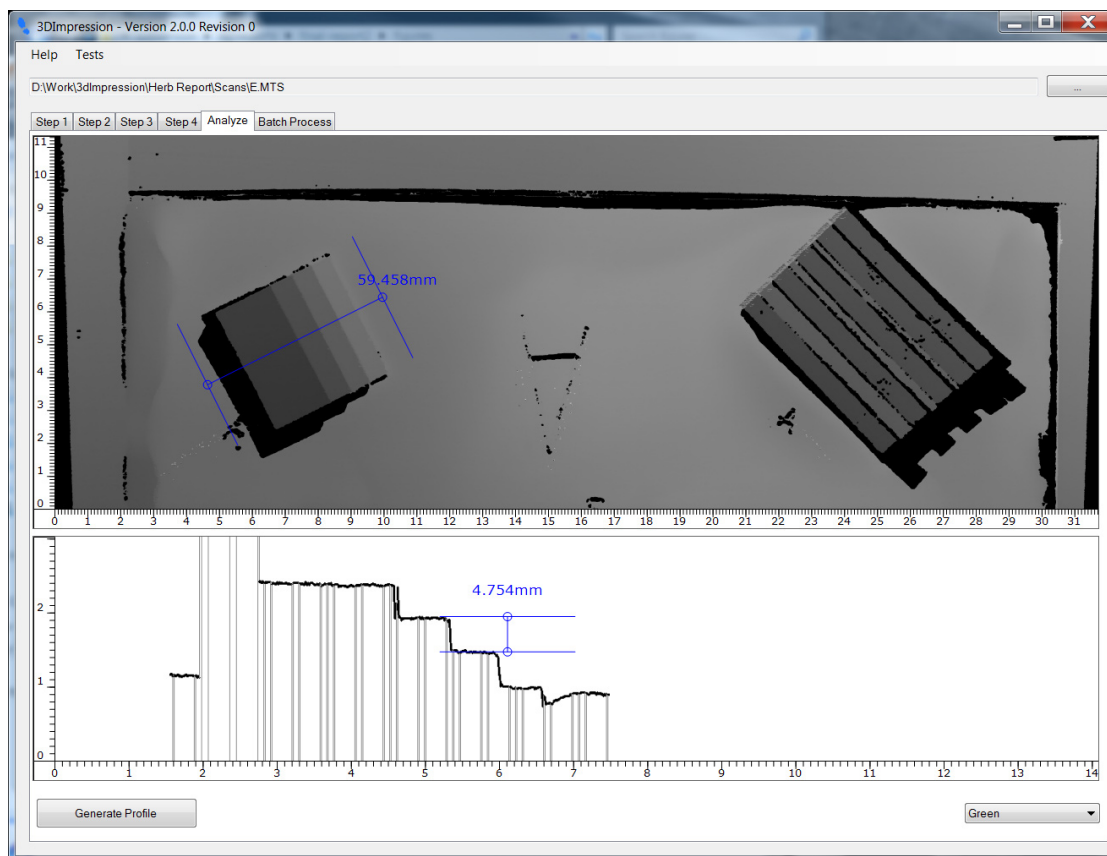


Figure A.4.: The graphical user interface to capture 3D measurements.

APPENDIX B COOL MUSCLE PROGRAM

Cool Muscle CM1 is a programmable motor. It has four inputs and two outputs. A program is developed to home, to move, to stop, based on the state of the four inputs. The program is as follows. Default parameter setting code is excluded.

```
/set ID to motor 1
.1

/set variables
V1=0
V3=0
V2=2
V4=4
V8=8

/set the logic scan time
K87=5

/set logic bank on power up
K85=1

/clear all program banks
B100

/clear all logic banks
L100

/set starting position
P1=-1000
```

```

/set short run position
P2=-40000

/set long run position
P3=-130000

/set default values
P0=-1000
S0=4
A0=100
M0=100
N0=0
R0=0
S1=4
A1=100

L1.1
/calculate value set by input
V0=I1;
V1=I2*V2;
V0=V0+V1;
V1=I3*V4;
V0=V0+V1;
V1=I4*V8;
V0=V0+V1;
/computed V0 is compared to 0
/if 0 goto start(T0)
/else goto L2.1
V0!=V3,CL2,T0;
END.1

L9.1

```

```
V0=I2;
V0==N0 ,] ,CL4;
END .1
/if input#1 is 0 stop.
/else call L3
L2 .1
V3=V0;
V0==N1 ,] ,CL3;
END .1

L3 .1
V0==N2 ,CL4 ,T0;
V0==N4 ,CL5 ,T0;
V0==N8 ,CL6 ,T0;
END .1

/execute bank 1
L4 .1
[1 .1
END .1

/execute bank 3
L5 .1
[3 .1
END .1

/execute bank 4
L6 .1
[4 .1
END .1
```

```
/home (bank 1)
B1.1
|
|2
S1,A1,P1
END.1

/stop (bank 2)
B2.1
].1
END.1

/short run (bank 3)
B3.1
S1,A1,P2
END.1

/long run (bank 4)
B4.1
S1,A1,P3
END.1

/save data to eeprom
$.1
```